



Full Titel of the Paper
Guidelines for Preparation of Paper Manuscripts
for the 12th - Japanese-German Bridge Symposium, Munich, Germany, 4.9. - 7.9.2018

Univ. Prof. Dr.-Ing. Werner Mustermann *
Dipl.-Ing. Dr. h.c. mult. Alois Fipps **

* Technische Universität München, Chair of Construction, Germany, w.mustermann@tum.de

** Fipps - Engineering GmbH & CoKG, Bonn, Germany, a.fipps@engineering.com

Abstract

Try to keep the abstract within 10 lines. Please, do not have references or displayed equations in the abstract.

Keywords: Three to five keywords should be typed here (Times New Roman 10 pt bold)

1 Introduction

Text (Times New Roman, 10 pt, line spacing 1,0, justification)

The length of each manuscript of the paper should be in the range of about 4 to 12 pages. It is advised to use the full space allocated for each paper. The manuscript must be typed on A4 sheets (length: 297 mm; width: 210 mm). The left and right margins as well as the top and bottom margins should be 20 mm. The typing area of each page is 252 x 170 mm. All text and artwork (including figure captions) should be placed within this area. Do not leave any unnecessary space. The page numbering will be added later by the publisher. The SI-system of units should be used in the paper.

Please note:

We received about 75 papers for a contribution to the 12th JGBS. The full paper of each contribution will be published in the symposium proceedings on a CD and an abstract in printed form. For the symposium proceedings, please send us your full paper and additionally an extended abstract **in a range of 2 pages**. Please use for the full paper as well as the extended abstract the guidelines “format-JGBS”.

Please note that the final deadline for submitting your full paper and the extended abstract is July 15th, 2018. Your files should be Microsoft Word documents, with the following filenames:

For the paper: PAP<first author name>, e.g. PAPmustermann.doc

For the abstract: ABS<first author name>, e.g. ABSmustermann.doc

The electronic files may be submitted by one of the following two methods,

1. If the file size is less than 10 MB the file may be sent as an attachment via email to: paper@jgbs.de
2. Files can be sent on CD-ROM by mail to the
University of the German Armed Forces.
Institut für Konstruktiven Ingenieurbau
c/o Dr.-Ing. E. Hiller
Werner-Heisenberg-Weg 39
85577 Neubiberg - Germany

2 Typing

The text should be typed in BLACK colour, and font should be Times New Roman, if not possible a similar font. The use of 10 point font and single line space for main text of paper is strongly recommended. Type the title on the top of the first page. There is one empty line space between the title of the paper and the author(s), one empty line space between the author(s) and the affiliation(s) of author(s), and one empty line space between the main headings.

2.1 Title: (Headline 2; Times New Roman 10 pt)

The Title of the paper should be typed in upper and lower case with 12 point bold typeface. The title should be centered.

2.2 Author's name

Type the author's name(s) with 10 point bold typeface and in the order of first, middle and last name. There is one empty line above and below the name(s) of the author(s). The author's name(s) should be centered.

2.3 Affiliation

The affiliation(s) of the author(s) (including city, country and e-mail address) should be typed below the list of authors. The affiliation(s) should be centered and typed with 10 point normal typeface.

2.4 Abstract

Try to keep the abstract within 10 lines. Please, do not have references or displayed equations in the abstract. There should be one empty line between the abstract and the affiliation(s) of the author(s).

2.5 Key Words

The key words are necessary for each paper. Try to keep the number of words within five. There is one empty line space below the key words.

2.6 Headlines

The main headlines should be numbered as 1., 2., 3. with 10 point bold typeface and start from left end of line. A main headline should have one line space above.

The second headlines, if necessary, should be typed with 10 point normal typeface and should be numbered as 1.1, 1.2, 1.3. There is one line space above the secondary headline, but no space below it.

2.7 Equation

All equations must be set or clearly typed and continuously numbered. All equations should be centered. Displayed equations should be numbered as (1), (2), (3). The numbers should appear at the right of the line in parentheses. Refer to equations in the text as Eq. (1), Eq. (2).

$$M_{Ki,y} = \xi \cdot N_{Ki,z} \cdot \left[\sqrt{(c^2 \cdot 0,25 z_p^2) + 0,5 z_p} \right] \quad (1)$$

2.8 Tables and Figures

All tables and figures should be continuously numbered. Please arrange the table titles above the tables and the figure captions below the figures. Allow one line space between the table and its title and the figures and its caption. Allow one line space between the table or figure and the adjacent text. Table(s) should be three-line table(s). In figures the line symbols need to be in a manner that a clear distinction is possible in black-and-white representation.

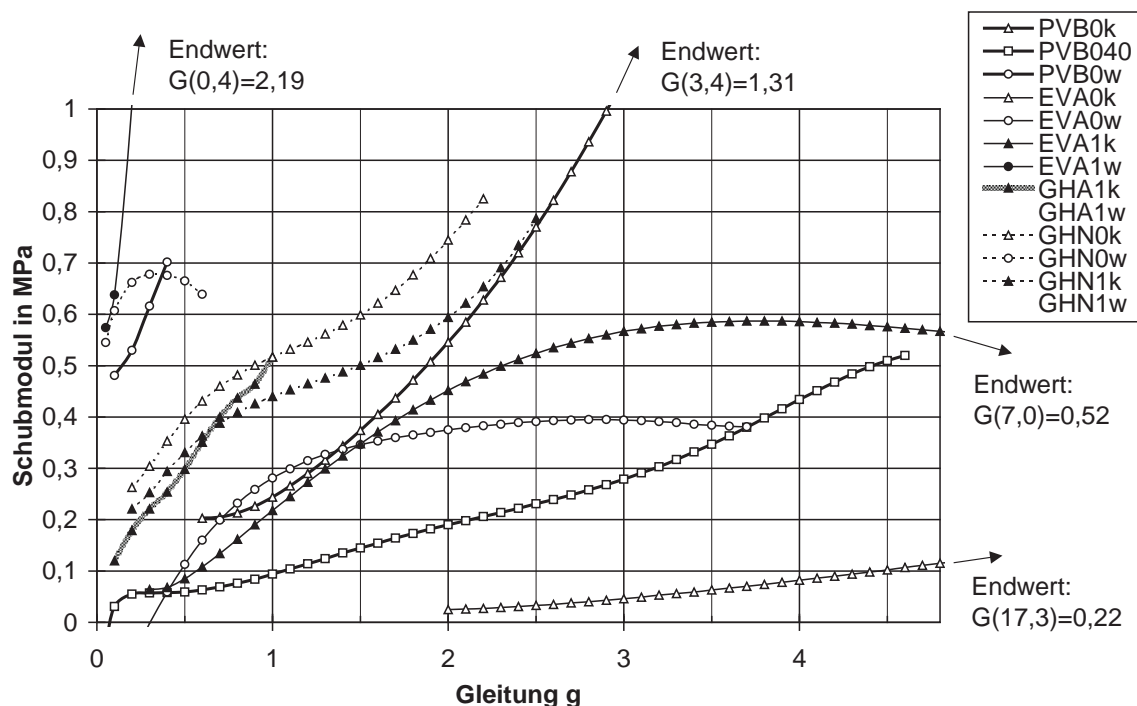


Figure 1: Shearing strain g

3 References

References should be shown in the text as [1, 2, 4, 5, 7-9]. Prepare an appendix listing all references in chronological order according to the following examples.

Table 1: Deflection limit values for single span girders referring to actions from operating and environment

Direction	Load case	Deformation at $x = 0,5 \cdot L_{St}^*$	Action	Limit value min L_{St}^* / max w	Limit value max ϕ_y at $x = 0$
Vertical (z-direction)	Traffic (vehicle)	max w_{Fzg}	stat $p_{z,Fzg} = 20,4 \text{ kN/m}$	+ 2400	$\pm 6,000 \cdot 10^{-4}$
			stat $p_{y,Fzg} = 2,9 \text{ kN/m}^{**}$		
	Temperature	max $w_{\Delta T}$	$t_o > t_u$	- 4500	$\pm 4,215 \cdot 10^{-4}$
			$t_o < t_u$	+ 4400	$\pm 3,201 \cdot 10^{-4}$
Horizontal (y-direction)	Traffic (vehicle)	max v_{Fzg}	stat $p_{y,Fzg} = 2,9 \text{ kN/m}$	± 12000	$\pm 1,255 \cdot 10^{-4}$
	Temperature	max $v_{\Delta T}$	$t_l > t_r$ $t_l < t_r$	± 4800	$\pm 4,215 \cdot 10^{-4}$

Table 2: Deflection limit values for single span girders referring to actions from operating and environment

Direction	Load case	Deformation at $x = 0,5 \cdot L_{St}^*$	Action	Limit value min L_{St}^* / max w	Limit value max ϕ_y at $x = 0$
Vertical (z-direction)	Traffic (vehicle)	max w_{Fzg}	stat $p_{z,Fzg} = 20,4 \text{ kN/m}$	+ 2400	$\pm 6,000 \cdot 10^{-4}$
			stat $p_{y,Fzg} = 2,9 \text{ kN/m}^{**}$		
	Temperature	max $w_{\Delta T}$	$t_o > t_u$	- 4500	$\pm 4,215 \cdot 10^{-4}$
			$t_o < t_u$	+ 4400	$\pm 3,201 \cdot 10^{-4}$
Horizontal (y-direction)	Traffic (vehicle)	max v_{Fzg}	stat $p_{y,Fzg} = 2,9 \text{ kN/m}$	± 12000	$\pm 1,255 \cdot 10^{-4}$
	Temperature	max $v_{\Delta T}$	$t_l > t_r$ $t_l < t_r$	± 4800	$\pm 4,215 \cdot 10^{-4}$

4 Introduction

Some radio-frequency (RF) waves in the frequency range from MHz to GHz are observed during the period of neutral beam injection (NBI) in Large Helical Device (LHD) plasmas [1-3]. Frequency spectra obtained near the perpendicular NBI ports show that there are some peaks near the ion cyclotron frequency and its harmonics; the ion cyclotron emissions (ICEs) are localized near the perpendicular NBI ports [1, 2]. In addition to the ICEs, RF waves in the Lower Hybrid Wave (LHW) frequency region are detected during the perpendicular NBI [3]. These waves are not localized near the NBI ports and have frequencies increasing with the plasma density.

Both the ICEs with $\omega \simeq l\Omega_i$, where l is an integer and Ω_i is the ion cyclotron frequency, and the RF waves in the LHW frequency region, $\omega \sim \sqrt{\Omega_i\Omega_e}$, where Ω_e is the electron cyclotron frequency, can be excited by energetic ions produced by the perpendicular NBI. The velocity distribution of the energetic ions produced by the NBI may be approximated by a ring-like distribution in the velocity space perpendicular to the magnetic field. According to linear theories on instabilities driven by such a ring-like distribution, ion cyclotron harmonic waves with $\omega \simeq l\Omega_i$ can be destabilized [4, 5]. The lower hybrid waves with $\omega \sim \sqrt{\Omega_i\Omega_e}$ can be also excited by a ring-like distribution because of the interaction between the waves and the energetic-ion beam across the magnetic field [6]. If the speed of the energetic ions is smaller than the Alfvén speed v_A , the energetic ions can interact with the high-frequency magnetosonic waves with $\omega \sim \sqrt{\Omega_i\Omega_e}$ propagating perpendicularly or quasi-perpendicularly to the magnetic field. This may be an excitation mechanism for RF waves of the LHW range observed in the LHD.

In this paper, we study instabilities of high-frequency magnetosonic waves driven by an ion ring-like distribution using an electromagnetic particle in cell (PIC) code. We perform simulations for typical parameters for LHD plasmas and investigate linear and nonlinear evolution of the high-frequency magnetosonic waves with $\omega \sim \sqrt{\Omega_i\Omega_e}$ excited in association with the ICEs. We also discuss how the frequencies of the excited magnetosonic waves depend on the plasma density.

5 Simulation Model and Parameters

We use a one-dimensional (one spatial coordinate and three velocity components), electromagnetic, particle-in-cell (PIC) code, which self-consistently simulates full dynamics of electrons and ions and evolution of electromagnetic fields, using the full Maxwell's equations and the equations of motion of particles. This enables us to consider both ICEs with $\omega \simeq l\Omega_i$ and instabilities of high-frequency magnetosonic waves with $\omega \sim \sqrt{\Omega_i\Omega_e}$ including kinetic effects of ions and electrons. The plasma consists of three components: minority energetic ions, electrons, and bulk ions. Initially, the electrons and bulk ions have Maxwell velocity distributions, whereas the energetic ions have a ring-like distribution in the velocity space with $v_{\parallel} = 0$, which is given by

$$f(v_{\parallel}, v_{\perp}) = \delta(v_{\parallel})\delta(v_{\perp} - u)/(2\pi u), \quad (2)$$

where v_{\parallel} and v_{\perp} are velocities parallel and perpendicular to the external magnetic field, respectively, and u is the initial perpendicular speed of the energetic ions.

We assume that the external magnetic field is uniform because we consider waves with wavelengths shorter than several centimeters and the variation of the LHD magnetic field for these lengths is negligibly small (the ratio of the variation to the total strength is less than several percent). The waves propagate in the x direction in the external magnetic field $\mathbf{B}_0 = (B_0 \cos \theta, 0, B_0 \sin \theta)$, where θ is the propagation angle of the waves. Setting $\theta \simeq 90^\circ$, we simulate the waves propagating perpendicularly or quasi-perpendicularly to \mathbf{B}_0 . The simulation system is periodic in the x direction with the length $L_x = 4096\Delta_g$, where Δ_g is the grid spacing, and the electron skin depth is $c/w_{pe} = 10\Delta_g$, where w_{pe} is the electron plasma frequency; the system length corresponds to several tens of centimeters if the plasma density is $n \sim 10^{19} \text{ m}^{-3}$. The ion-to-electron mass ratio is $m_i/m_e = 3672$ for Deuterium (D). The total number of simulation particles is of order 10^7 . The total charge of the electrons is equal to that of the ions. The density ratio of the energetic ions to the bulk ions is $n_h/n_i = 10^{-2}$. To have good statistics for the energetic ions with the low density, we use the method of fine particles (for example, see Ref. [7]). Keeping the mass-to-charge ratio of the energetic ions unchanged, we take the mass and charge of the energetic ions to be small and increase the number of the energetic ions by 10 times, which leaves the energetic-ion mass density, plasma frequency, and cyclotron frequency unchanged. The time step is $\omega_{pe}\Delta t = 0.05$. We calculate the evolution of the plasma and the electromagnetic fields for about five times as long as the ion cyclotron period.

We set other simulation parameters by considering the typical parameters for the edge of the LHD plasma, at which the ICEs can be excited [3]. The ratio of the light speed to the electron thermal speed is $c/v_{Te} = 70$, indicating that the electron temperature $T_e \sim 100 \text{ eV}$. The bulk ion temperature is equal to the electron temperature. The strength of the external magnetic field is $B_0 = 1.57 \text{ T}$. We show the results of the cases for various plasma densities. The values of Ω_e/w_{pe} , the Alfvén speed v_A , and the ratio of the energetic ion speed u to v_A vary with the plasma density.

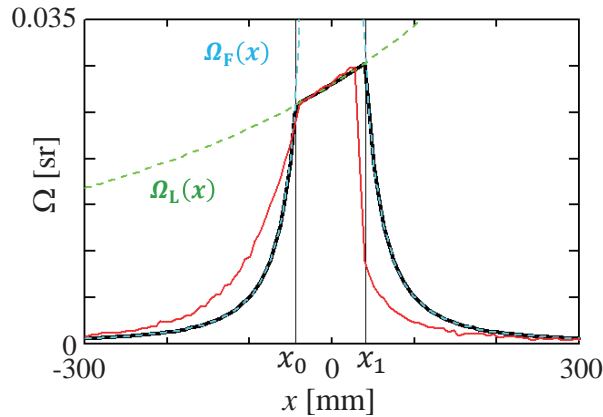


Figure 2: Power spectrum of magnetic fluctuations in a thermal equilibrium Deuterium (D) plasma.

6 Simulation Results

6.1 Magnetic fluctuations

We firstly present a simulation result for magnetic fluctuations in a thermal equilibrium plasma without energetic ions. Figure 1 shows the power spectrum $P(k, \omega)$ of magnetic fluctuations with $\theta = 89.5^\circ$ in a Deuterium (D) plasma with the electron density $n_e = 10^{19} \text{ m}^{-3}$ and the external magnetic field $B_0 = 1.57 \text{ T}$. The value of Ω_e/w_{pe} is 1.54 and the plasma beta is 2×10^{-4} . The color on Fig. 1 indicates the amplitudes of the magnetic fluctuations. We can see that the amplitudes

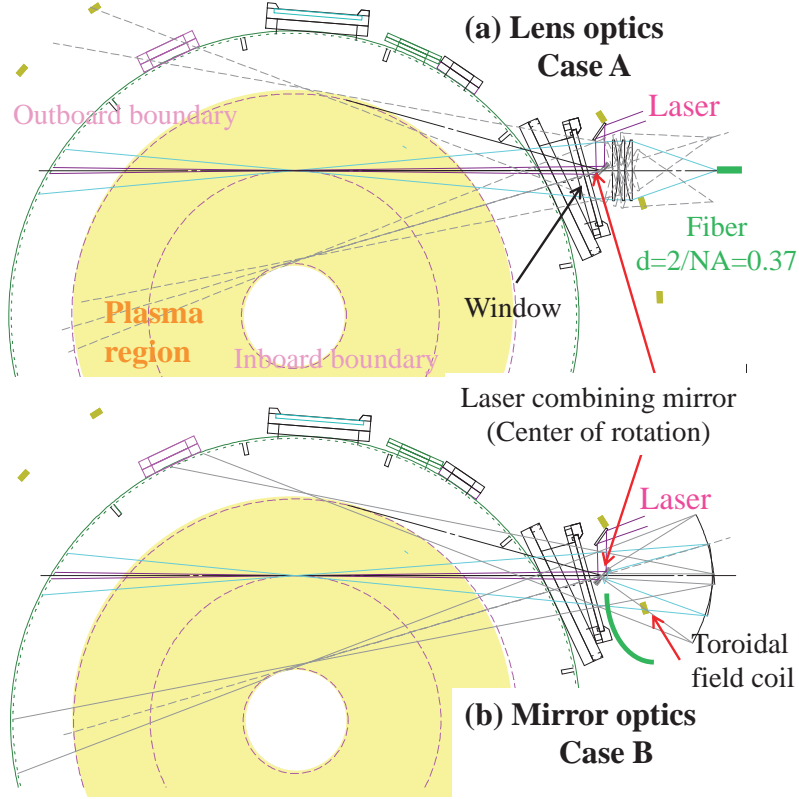


Figure 3: Power spectrum of magnetic fluctuations in a D plasma with energetic ions with a ring-like velocity distribution.

are great along the dispersion curve of the magnetosonic wave given by

$$\omega_{\text{mg}} = \frac{v_A k}{[1 + (c^2 k^2 / \omega_{\text{pe}}^2)(1 + \Omega_e^2 / \omega_{\text{pe}}^2)]^{1/2}}, \quad (3)$$

where θ is approximated as $\theta = 90^\circ$. The resonance frequency of the perpendicular magnetosonic wave is the lower-hybrid resonance frequency defined as

$$\begin{aligned} \omega_{\text{LH}} &= \sqrt{\Omega_i \Omega_e [(1 + \Omega_i^2 / \omega_{\text{pi}}^2) / (1 + \Omega_e^2 / \omega_{\text{pe}}^2)]^{1/2}} \\ &= \Omega_i \Omega_e [(1 + \omega_{\text{pi}}^2 / \Omega_i^2) / (\omega_{\text{pe}}^2 + \Omega_e^2)]^{1/2}. \end{aligned} \quad (4)$$

The magnetic fluctuations of ion cyclotron waves with $\omega \simeq l\Omega_i$ are much smaller than those of the magnetosonic waves because the plasma beta is very low [8].

Next, we show the magnetic fluctuations in a D plasma with energetic ions in Fig. 2, where the initial speed of the energetic ion is $u = 0.31v_A$, which corresponds to the speed of the D ions with the energy $K = 60 \text{ keV}$ in the D plasma with $n_e = 10^{19} \text{ m}^{-3}$ and $B_0 = 1.57 \text{ T}$. Comparing this with Fig. 1, we see that super-thermal magnetic fluctuations are near the D cyclotron frequency and its harmonics, $\omega \simeq l\Omega_D$. These are the ICEs due to the energetic ions. Further, the magnetosonic waves with frequencies slightly smaller than ω_{LH} have large amplitudes. These high-frequency magnetosonic waves are also excited by the energetic ions.

Figure 3 shows the frequency spectra $P(\omega)$ of the magnetic fluctuations for the wavenumbers $kv_A/\Omega_D = 2.8$ (a) and $kv_A/\Omega_D = 61.5$ (b) and the time variations of the amplitudes of the fluctuations for these wavenumbers (c). In Fig. 3 (a), there are four peaks at $\omega/\Omega_D \simeq 1, 2, 3$, and 2.8 . The last peak is the magnetosonic wave. The former three peaks are the ion cyclotron waves supported by the energetic ions [5]; they are not the Bernstein modes due to the bulk ions and can exist in the limit of a cold energetic-ion beam given by eq. (1). As shown by the red line in Fig. 3 (c), those waves are saturated at about the ion cyclotron period $\Omega_D t \simeq 2\pi$. The peak in Fig. 3 (b) is the high-frequency magnetosonic wave with the frequency slightly smaller than ω_{LH} . The black line in Fig. 3 (c) shows that in the early stage $\Omega_D t < 4$, the high-frequency magnetosonic wave (b) grows faster than the low frequency modes (a) although there are small fluctuations of a period much shorter than the ion cyclotron period. The amplitude of the high-frequency magnetosonic wave is also saturated by the ion cyclotron period.

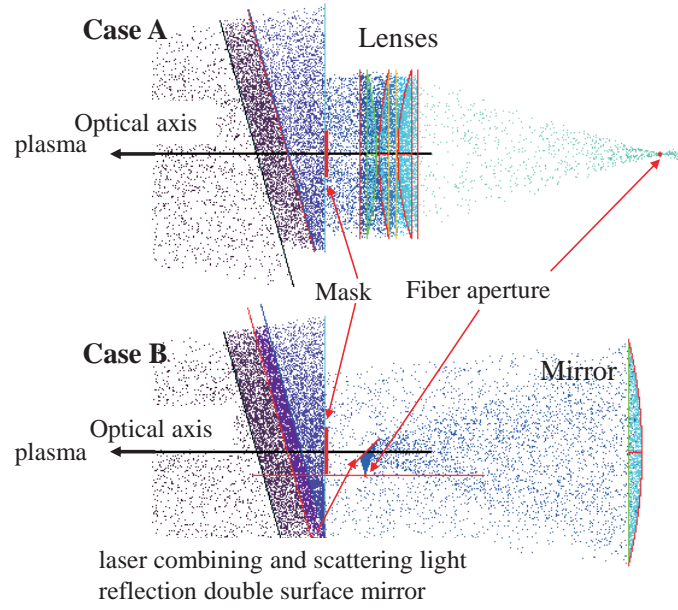


Figure 4: Frequency spectra of the magnetic fluctuations for $kv_A/\Omega_D = 2.8$ (a) and 61.5 (b) and time variations of their amplitudes (c).

Figure 4 shows the time evolution of velocity distribution functions of $f(v_\perp)$ and $f(v_x)$ of the energetic ions. The distribution functions are drastically changed by the time $\Omega_D t = 6$ because the energies are rapidly transferred from the energetic ions to the waves through the instabilities, which causes the saturation of the waves, as shown in Fig. 3.

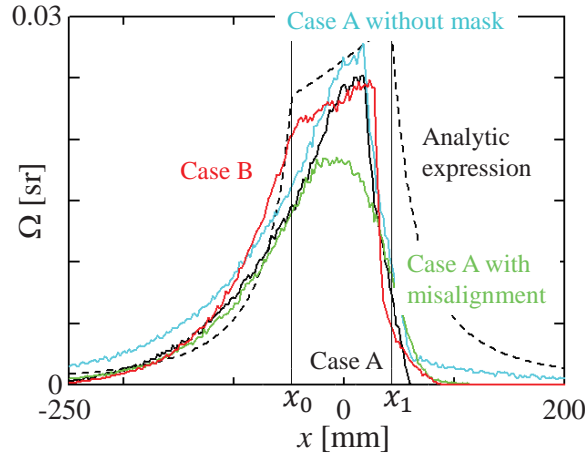


Figure 5: Time evolution of velocity distributions $f(v_\perp)$ and $f(v_x)$ of the energetic ions.

6.2 Comparison with linear theory

We compare the simulation results with a linear theory on instabilities of high-frequency magnetosonic waves. Because the wave frequencies are much higher than the ion cyclotron frequency and the waves are saturated by the ion cyclotron period, we assume that the energetic ions are unmagnetized. Then, we can approximate the energetic ions that can interact with the waves propagating in the x direction as the energetic ion beams with the initial velocity $\mathbf{v} = (\pm u, 0, 0)$. Based on the three-fluid (electrons, ions, and energetic beam) model [9], we can obtain a linear dispersion relation for the high-frequency magnetosonic waves interacting with the positive beam with $v_x = u$ as

$$\omega^2 - \omega_{\text{mg}}^2 - \frac{\omega_{\text{ph}}^2}{\omega_{\text{pi}}^2} \frac{\omega_{\text{mg}}^4}{(\omega - ku)^2} = 0, \quad (5)$$

where ω is the complex frequency, ω_{mg} is given by eq. (3), and ω_{ph} and ω_{pi} are the plasma frequencies of the energetic ions and bulk ions, respectively.

We consider the solution of eq. (5), $\omega = \omega_r + i\gamma$, near $\omega_r = \omega_{\text{mg}}$, where ω_r is the real frequency and γ is the growth rate. We can expect from eqs. (3) and (5) that the real frequency ω_r increases with k and the growth rate γ becomes maximum

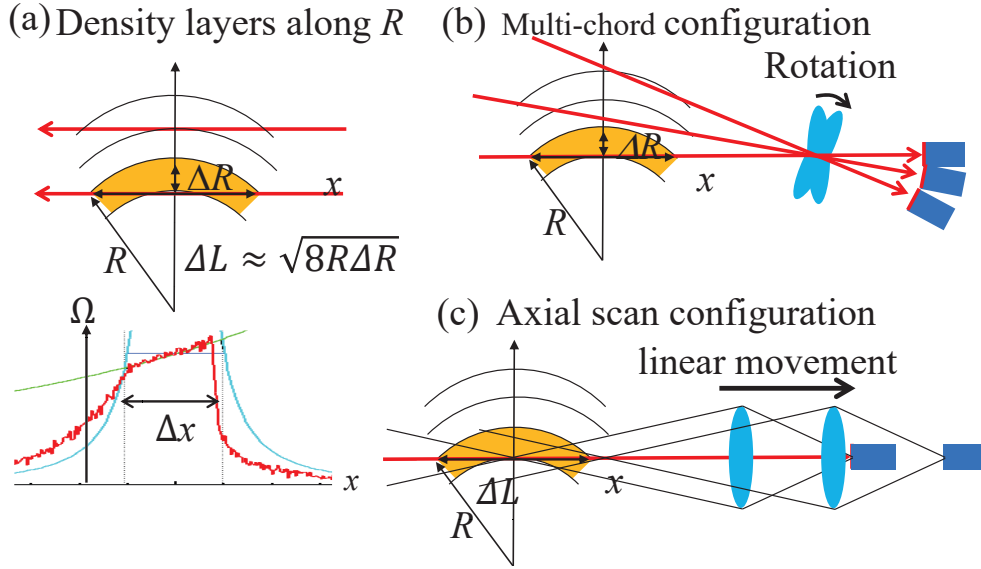


Figure 6: Growth rate γ of the high-frequency magnetosonic wave as a function of real frequency ω_r obtained by the linear theory. The real frequency of the most unstable mode is written as ω_{rm} .

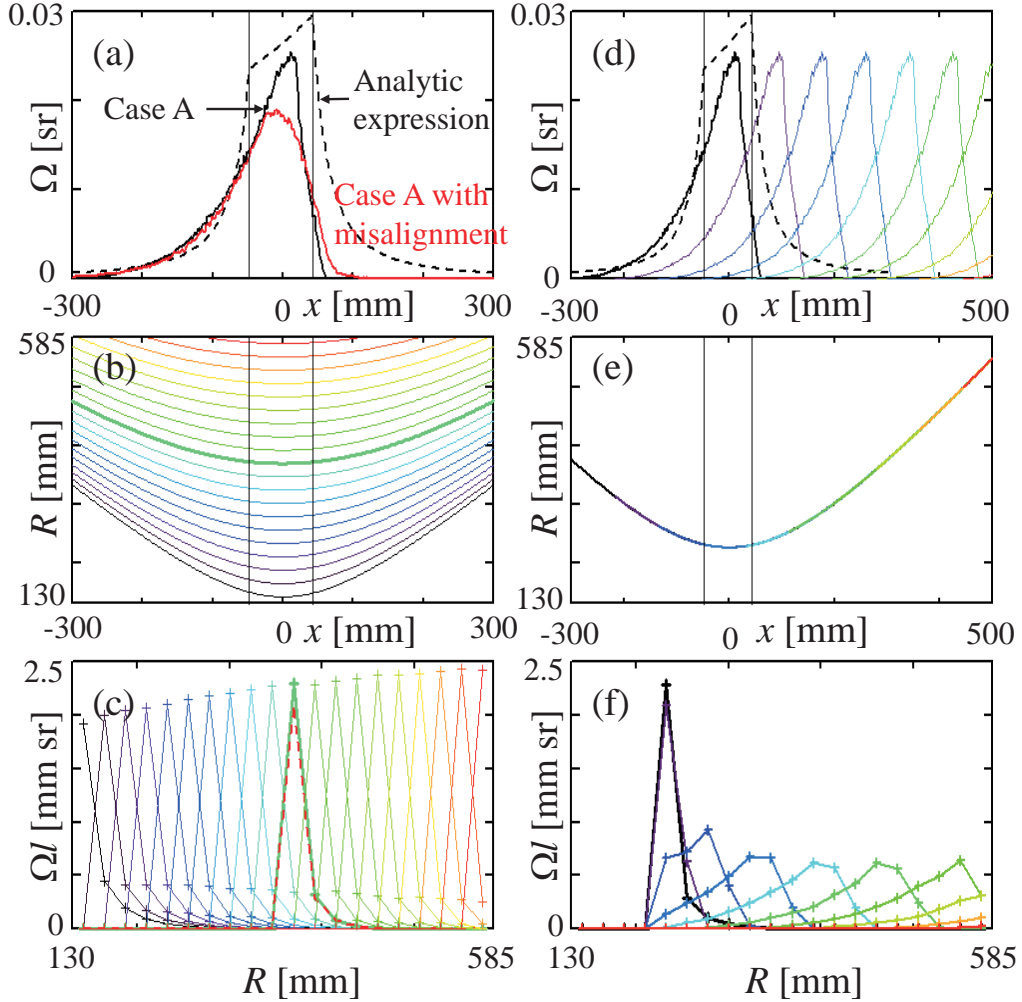


Figure 7: Frequencies of the mode with the largest amplitude in the simulation and of the most unstable mode predicted by the linear theory as functions of the electron density.

near the wavenumber satisfying the relation $\omega_{mg} = ku$. That is, γ becomes maximum near the real frequency ω_r at this wavenumber if γ is expressed as a function of ω_r . We write the real frequency of the most unstable mode as ω_{rm} . Figure

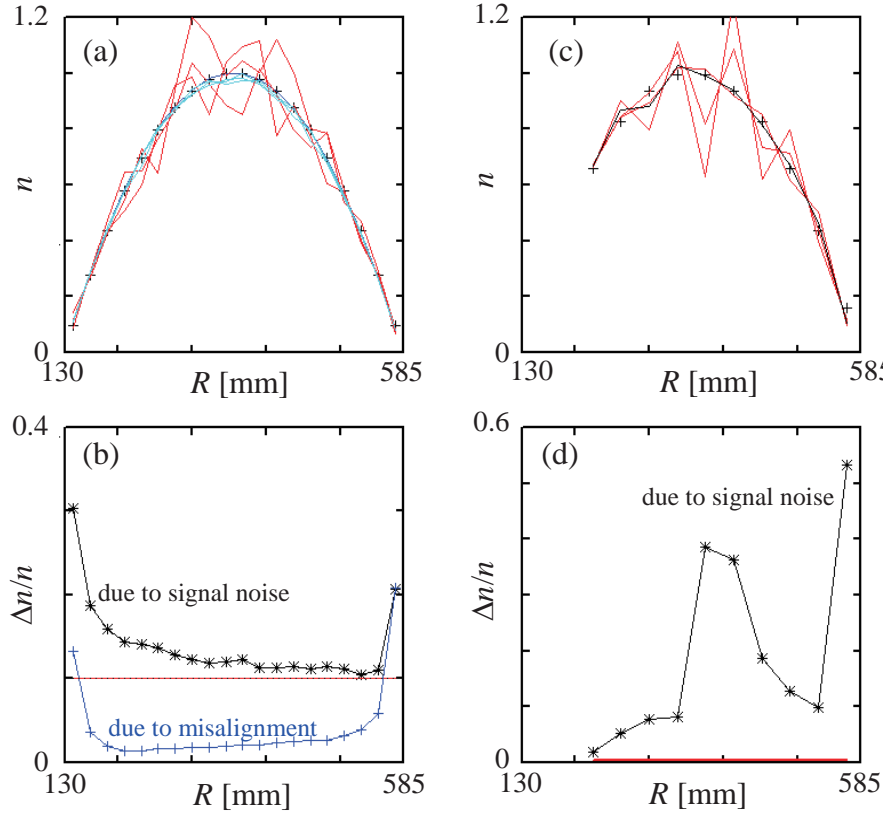


Figure 8: Frequency spectra of magnetic fluctuations in high density plasmas. The vertical gray lines show the frequencies of the most unstable modes predicted by the linear theory.

5 shows the result of the numerical calculation of eq. (5) for the same values of B_0 , n_e , and u/v_A as for Fig. 2. This figure indicates that the frequency of the most unstable mode is $\omega_{rm} \approx 30\Omega_D$. The theoretical frequency ω_{rm} is in good agreement with the simulation result shown in Fig. 2, where the amplitude is the largest at $\omega \approx 30\Omega_D$. The theoretical growth rate of the most unstable mode is $\gamma \approx 2\Omega_D$, which is about twice as large as the growth rate shown by the black line in Fig. 3, $\gamma \approx \Omega_D$ for the period from $\Omega_D t = 2$ to 3; the smaller growth rate in the simulation can be due to effects not included in the linear theory, such as kinetic effects of electrons and bulk ions and effects of change in the velocity distribution of the energetic ions.

6.3 Density dependence

According to the LHD experimental results, the frequency of the RF waves of the LHW range increases with the line-averaged electron density when the density is smaller than $2 \times 10^{19} \text{ m}^{-3}$ [3]. In order to study the density dependence of instabilities of the high-frequency magnetosonic waves, we perform simulations for various electron densities, keeping the external magnetic field $B_0 = 1.57 \text{ T}$, the energy of the energetic ions $K = 60 \text{ keV}$, and the propagation angle of the waves $\theta = 90^\circ$.

Figure 6 shows the frequency of the magnetosonic wave that has grown to the largest amplitude as a function of the electron density, where the dots are the simulation results and the dashed and solid lines represent the lower hybrid resonance frequency ω_{LH} given by eq. (4) and the frequency of the most unstable mode ω_{rm} predicted by the linear theory (5). The simulation results are in good agreement with the linear theory. Both the theory and simulations show that the frequency of the magnetosonic wave increases with the electron density. The tendency that the frequency increases with the density is the same as that in the LHD experiments on the RF waves in the LHW frequency region. The right axis of Fig. 6 shows that the frequencies of the magnetosonic waves are of the order of 100 MHz, which are the same order as the frequencies of the RF waves of the LHW range observed in the LHD.

Figure 7 shows the results for the cases of $n_e \geq 2 \times 10^{19} \text{ m}^{-3}$, where the frequency spectra for $n_e (10^{19} \text{ m}^{-3}) = 2, 4, 6$, and 8 obtained by the simulations (black lines with triangles) and the frequencies of the most unstable mode given by the linear theory ω_{rm} (gray vertical lines) are shown. When $n_e > 2 \times 10^{19} \text{ m}^{-3}$, the frequency of the dominant mode does not always increase with n_e .

We thus showed that the frequency of the magnetosonic wave excited by the energetic ions with a ring-like distribution

increases with the electron density when the density is relatively small. This qualitatively agrees with the LHD experimental results on RF waves of LHW range, although there is a discrepancy in the density (the density at the excitation position is used in the simulation, whereas the line-averaged electron density is used in the LHD experiments).

7 Summary

By means of a one-dimensional electromagnetic particle in cell code, we have studied instabilities of high-frequency magnetosonic waves caused by energetic ions with a ring-like distribution in the velocity space perpendicular to the magnetic field. We have performed simulations for typical parameters for the LHD experiments.

We have shown that the magnetosonic waves with frequencies slightly smaller than the lower-hybrid resonance frequency grow to large amplitudes, in addition to super-thermal ICEs. These waves are saturated by the ion cyclotron period because of the change in the velocity distribution of the energetic ions. The frequency of the magnetosonic wave that has grown to the largest amplitude is in good agreement with the frequency of the most unstable mode predicted by a linear theory. The theory and simulations have shown that the frequency of the magnetosonic wave increases with the plasma density when the density is relatively small, which qualitatively agrees with the LHD experimental results on RF waves of the LHW range observed during the perpendicular NBI.

Acknowledgments

This work is performed with the support and under the auspices of the NIFS Collaboration Research program (NIFS16 KNXN337).

8 References

- [1] K. Saito *et al.*, Fusion Eng. Des. **84**, 1676 (2009).
- [2] K. Saito *et al.*, Plasma Sci. Technol. **15**, 209 (2013).
- [3] K. Saito *et al.*, ‘RF wave detection with high-frequency magnetic probes in LHD’, submitted to Plasma Fusion Res.
- [4] V.S. Belikov and Ya. I. Kolesnichenko, Sov. Phys. Tech. Phys. **20**, 1146 (1976).
- [5] R.O. Dendy *et al.*, Phys. Plasmas **1**, 3410 (1994).
- [6] K.A. Akimoto *et al.*, J. Plasma Phys. **34**, 445 (1985).
- [7] M. Toida and Y. Ohsawa, Solar Phys. **171**, 161 (1997).
- [8] M. Toida, Y. Yoshiya and Y. Ohsawa, Phys. Plasmas **12**, 102306 (2005).
- [9] D.W. Ross, Phys. Fluids **13**, 746 (1970).